

## Impact of GVF Derivation Methods on Noah Land Surface Model Simulations and WRF Model Forecasts

LI FANG

*Earth System Science Interdisciplinary Center, University of Maryland, College Park, and NOAA/NESDIS/STAR, College Park, Maryland*

XIWU ZHAN

*NOAA/NESDIS/STAR, College Park, Maryland*

CHRISTOPHER R. HAIN

*NASA Marshall Space Flight Center, Huntsville, Alabama*

JIFU YIN AND JICHENG LIU

*Earth System Science Interdisciplinary Center, University of Maryland, College Park, and NOAA/NESDIS/STAR, College Park, Maryland*

(Manuscript received 19 April 2018, in final form 19 August 2018)

### ABSTRACT


Green vegetation fraction (GVF) plays a crucial role in the atmosphere–land water and energy exchanges. It is one of the essential parameters in the Noah land surface model (LSM) that serves as the land component of a number of operational numerical weather prediction models at the National Centers for Environmental Prediction (NCEP) of NOAA. The satellite GVF products used in NCEP models are derived from a simple linear conversion of either the normalized difference vegetation index (NDVI) from the Advanced Very High Resolution Radiometer (AVHRR) currently or the enhanced vegetation index (EVI) from the Visible Infrared Imaging Radiometer Suite (VIIRS) planned for the near future. Since the NDVI or EVI is a simple spectral index of vegetation cover, GVFs derived from them may lack the biophysical meaning required in the Noah LSM. Moreover, the NDVI- or EVI-based GVF data products may be systematically biased over densely vegetated regions resulting from the saturation issue associated with spectral vegetation indices. On the other hand, the GVF is physically related to the leaf area index (LAI), and thus it could be beneficial to derive GVF from LAI data products. In this paper, the EVI-based and the LAI-based GVF derivation methods are mathematically analyzed and are found to be significantly different from each other. Impacts of GVF differences on the Noah LSM simulations and on weather forecasts of the Weather Research and Forecasting (WRF) Model are further assessed. Results indicate that LAI-based GVF outperforms the EVI-based one when used in both the offline Noah LSM and WRF Model.

### 1. Introduction

The Noah land surface model (LSM; Ek et al. 2003; Chen and Dudhia 2001) serves as the land component of a number of the operational numerical weather prediction (NWP) models at the National Centers for Environmental

Prediction (NCEP) of NOAA. Accuracy of the Noah LSM simulations directly affects the NWP models and may heavily rely on the accuracy of the input land surface parameters of the LSM. The green vegetation fraction (GVF) is one of the essential parameters, used as an important weighting coefficient in integrating the evaporation from both soil and vegetation surfaces and the vegetation transpiration into the latent heat flux between land surface and the atmosphere. The high sensitivity of the latent heat fluxes to the GVF value has been well documented (Abramopoulos 1988; Miller et al. 2006).

---

 Denotes content that is immediately available upon publication as open access.

---

Corresponding author: Li Fang, lfang1@umd.edu

DOI: 10.1175/JHM-D-18-0075.1

© 2018 American Meteorological Society. For information regarding reuse of this content and general copyright information, consult the [AMS Copyright Policy \(www.ametsoc.org/PUBSReuseLicenses\)](https://www.ametsoc.org/PUBSReuseLicenses).

Remotely sensed land vegetation indices (VIs) provide the capability of capturing the surface vegetation coverage and density globally and seasonally. The integration of a satellite-based GVF dataset into the LSM has made a significant improvement to the NCEP forecasts in the past decades (Gutman and Ignatov 1998; Zeng et al. 2003; Jiang et al. 2010; James et al. 2009; Miller et al. 2006; Ruhge and Barlage 2011; Yin et al. 2016). For instance, the climatological GVF datasets used in the operational NWP models at NCEP are derived from NOAA's Advanced Very High Resolution Radiometer (AVHRR) top-of-atmosphere normalized difference vegetation index (NDVI) as  $GVF = (NDVI - NDVI_{min}) / (NDVI_{max} - NDVI_{min})$ .  $NDVI_{min}$  and  $NDVI_{max}$  are predefined and are set as constants spatially and temporally (Gutman and Ignatov 1998). Their validation results showed that the use of the AVHRR-based GVF improved the predicted surface fluxes (Gutman and Ignatov 1998). Later on, Zeng et al. (2003) developed a fraction vegetation cover (FVC) dataset where  $NDVI_{min}$  is set at a global constant within each year but varies between years, while  $NDVI_{max}$  is a vegetation-type-dependent variable varying from year to year. Miller et al. (2006) analyzed the sensitivity of the Noah LSM to the FVC using the Zeng et al. (2003) approach. They found that the greatest impact on the surface energy and water balance appeared in the summer by increasing the transpiration more than  $10 \text{ W m}^{-2}$  on average. The above-mentioned satellite-based GVF inputs are average maps generated from multiyear satellite VI observations. The lack of the ability to capture real-time vegetation conditions in the GVF climatology dataset motivates the generation of a near-real-time (NRT) GVF for the use in NWP models (Jiang et al. 2010; James et al. 2009; Miller et al. 2006; Ruhge and Barlage 2011; Case et al. 2014; Yin et al. 2016). Jiang et al. (2010) derived weekly GVF based on AVHRR/NDVI from the operational global vegetation index system and further demonstrated the benefit of the NRT weekly GVF to NWP. Yin et al. (2016) examined the impact of both NRT albedo and GVF (NDVI based). They concluded that the use of NRT GVF improved Noah surface soil moisture (SM) simulations by 19.3% and soil temperature by 9.3%.

Although NDVI- or EVI-based GVF datasets have been operationally used in the numerical weather forecasting models for a wide range of applications, the issues and improvements are worth discussing. It is clear in the definition of a NDVI- or EVI-based GVF that it is not an intrinsic physical quantity. The main defect in radiometric remotely sensed VIs is the weak sensitivity to surface vegetation density changes when entering an asymptotic regime. It leads to saturation issues at moderate- to high-vegetation cases. Even though EVI is

designed to optimize the vegetation response with improved sensitivity in a high biomass region (Huete et al. 2002), the EVI-based GVF still suffers from the saturation problem at moderate to high values of the leaf area index (LAI; Fig. 3). Basically, spectral-based GVF is a description of how "green" a land pixel is when observed from a satellite sensor. It is based on the assumption that the green portion within the land pixel has uniform physical properties of the vegetation canopy. This means that evapotranspiration is not limited by the vertical density of vegetation on that green portion within the pixel, which is not always true in reality. In contrast, LAI, the ratio of the leaf surface area to unit ground surface area (Bégué 1993), is a more representative index of biophysical characteristics of vegetation. It is capable of representing the surface vegetation cover with respect to both horizontal cover and vertical densities. Thus, the GVF converted from LAI has the potential to more accurately describe the proportion of land surface and vegetation cover for biological and physical processes. However, the research on how the biophysical GVF would impact land surface models or even weather forecast models is limited. Therefore, the objectives of this paper are to 1) quantify the differences between spectrally based and biophysically based GVF and 2) evaluate their impacts on model estimates from both uncoupled Noah LSM and coupled weather forecast models [e.g., the Weather Research and Forecasting (WRF) Model].

Section 2 describes GVF derivation methods based on remotely sensed spectral and biophysical VIs, as well as relevant validation datasets. Models and experiment design are introduced in section 3. The differences between the two GVF datasets (EVI based and LAI based) and their impacts on offline Noah simulations and WRF forecasts are quantified in section 4. Section 5 provides the discussion and conclusions.

## 2. Datasets

### a. Green vegetation fraction

#### 1) GVF DATASETS BASED ON VEGETATION INDEX

Spatially distributed GVF data products can be derived from the vegetation index observed from satellite sensors. Some studies proposed a nonlinear relationship between spectral vegetation index and GVF (Carlson and Ripley 1997; Myneni and Williams 1994; Wittich 1997) while others suggested a linear relationship to be adequate (Gutman and Ignatov 1998). The derivation of GVF from vegetation indices usually involves the calculation of minimum VI for bare soil and maximum VI

for dense vegetation. The minimum and maximum VIs are empirically determined on the basis of analyses of a large set of data with spatial and temporal representativeness. The most common method to obtain the extreme values is to take the 5th and 95th percentiles from the probability distribution function of the global VI maps. Although NDVI-based GVF has been generated from many remotely sensed data (e.g., MODIS, AVHRR), the significant defect of the saturation issue is well known. Studies have shown that EVI is more responsive to canopy structural variation and better performs in heavy aerosol conditions (Huete et al. 2002; Gao et al. 2000). The official GVF product from Visible Infrared Imaging Radiometer Suite (VIIRS) sensors is being generated from EVI instead of NDVI, and the real-time EVI-based GVF product from VIIRS is planned to serve as inputs to NCEP operational Noah LSM runs in the future. This study, therefore, evaluates the EVI-based GVF as a representative of spectral-based VI.

The spectral GVF dataset is derived from the MODIS level-3 vegetation indices (MOD13A2; Huete et al. 1999). The EVI data in the MOD13A2 product are obtained at every 16 days at 1-km spatial resolution in the sinusoidal projection. The raw EVI tiles are smoothed and gap-filled based on quality control flags using the TIMESAT algorithm on a yearly basis (Jönsson and Eklundh 2002). The processed EVI tiles are then mosaicked to global maps at the original spatial resolution (1 km) using the MODIS Reprojection Tool (MRT). Last, the smoothed global EVI maps are converted to a GVF dataset based on the following linear transformation equation (Jiang et al. 2010):

$$\text{GVF} = (\text{EVI} - \text{EVI}_{\min}) / (\text{EVI}_{\max} - \text{EVI}_{\min}), \quad (1)$$

where  $\text{EVI}_{\min}$  and  $\text{EVI}_{\max}$  are theoretical EVI values for bare soil where  $\text{GVF} = 0$  and dense vegetation where  $\text{GVF} = 1$ . Both are global constants, independent of vegetation and soil types, and empirically estimated, following the current commonly used method. In our study, the statistics of  $\text{EVI}_{\max}$  and  $\text{EVI}_{\min}$  are set to 0.5707 and 0.0602, which are calculated by taking the 5th and 95th percentiles from the probability distribution function of global EVI maps at different seasons.

## 2) GVF DATASETS BASED ON LAI

A biophysical GVF dataset is derived from the level-4 MODIS global LAI and fraction of photosynthetically active radiation (FPAR) product (MOD15A2 V005), which is composited every 8 days at 1-km resolution (Knyazikhin et al. 1998, 1999).

The LAI product is produced by exploiting the MODIS spectral information of surface reflectance at up

to seven spectral bands. The main procedure of LAI derivation is based on a three-dimensional formulation of a radiative transfer algorithm in vegetation canopies. Meanwhile, a backup looking-table algorithm is triggered if the main procedure fails to estimate LAI using vegetation indices. The preprocess of raw LAI tiles is similar to that of spectral GVF introduced in section 2a(1) to keep their consistency. The raw LAI tiles are smoothed, gap-filled, and mosaicked to global maps at the original spatial resolution (1 km).

The processed global LAI maps are then converted to GVF dataset based on the following equation according to Norman's method (Norman et al. 1995):

$$\text{GVF} = 1 - e^{-b \times \text{LAI}}, \quad (2)$$

where  $b = 0.5$  is the extinction coefficient for general plant canopy.

## b. SM and weather datasets for validations

### 1) NORTH AMERICAN SOIL MOISTURE DATABASE

The North American Soil Moisture Database (NASMD), developed and constructed at the Department of Geography's Climate Science Laboratory at Texas A&M University, provides a harmonized and quality-controlled SM dataset for the entire continent of North America from a variety of networks, such as ARM Southern Great Plains, Climate Reference Network, Oklahoma Mesonet, SNOTEL, and many others (Quiring 2011). More details on NASMD can be found at <http://soilmoisture.tamu.edu/>. In this study, the accuracy of both surface and root-zone SM estimates from the long-term offline Noah LSM is validated using NASMD measurements. The top-layer measurements are used for surface SM validation, while the top  $N$  layers with the accumulated depth within 1 m are weighted averaged for root-zone SM comparison. Since NASMD combines ground observations from various networks,  $N$  may differ from site to site. There are eventually 593 NASMD sites in total involved in the validation process in this study.

### 2) GROUND WEATHER OBSERVATIONS FOR WRF FORECAST VALIDATION

The performance of WRF forecasts using different GVF inputs is assessed using ground weather observations of near-surface variables. Specifically, the Global Upper Air and Surface Weather Observations from NCEP are collected for the evaluation of surface and near-surface temperature and humidity forecasts. These observations are composed of a global set of surface and

upper-air reports operationally processed by NCEP, including pressure, geopotential height, temperature, dewpoint temperature, wind direction, and wind speed, with the time intervals ranging from hourly to 12 hourly. The data are archived in PREPBURF format available at the National Center for Atmospheric Research's Computational and Information Systems Laboratory (<http://rda.ucar.edu/datasets/ds337.0>).

### 3. Models and experiment designs

#### a. Models

##### 1) LIS AND THE NOAH LSM

The NASA Land Information System (LIS) is a flexible software framework to integrate satellite and ground-based observations and advanced LSMs to accurately characterize land surface states and fluxes (Kumar et al. 2006, 2008). The land surface modeling infrastructure in LIS consists of several well-documented LSMs (e.g., Noah, Community Land Model, Catchment, Mosaic), which typically run in an uncoupled mode using a combination of observation-based precipitation, radiation, and meteorological and land surface parameter datasets. The Noah LSM implemented in LIS is used in all experiments in this study because Noah LSM is the operational land surface model for the numerical weather prediction at NCEP (Ek et al. 2003; Chen and Dudhia 2001). It is a one-dimensional soil-atmosphere-vegetation transfer model which simulates four-layer soil moisture (both liquid and frozen) with thicknesses of 0–0.1, 0.1–0.4, 0.4–1, and 1–2 m (Chen et al. 1996; Chen and Dudhia 2001; Ek et al. 2003). Specifically, the Noah model, version 3.3, is employed in our study to test GVF's impact on offline model simulations, and it also serves as the core land component in the standard NCAR Advanced Research version of WRF (WRF-ARW) Model for forecasting.

##### 2) NASA NU-WRF

The NASA Unified WRF (NU-WRF) modeling system developed at the NASA Goddard Space Flight Center is an observation-driven integrated modeling system representing aerosol, cloud, precipitation, and land processes at satellite-resolved scales (Peters-Lidard et al. 2015). The NU-WRF (version 7) adopted in this study incorporates the standard WRF-ARW version 3.5.1 and LIS (v7.0rp1) into a unified framework with distinct advantages of 1) setting up long-term spinup land surface conditions on a common grid as the WRF forecast domain, 2) providing LIS land simulations with near-surface forcing from the parent WRF run, and 3) easy replacement of updated initial conditions from LIS

output to WRF. More details of NUWRF configurations are provided in section 3b(2).

#### b. Experiment design

A series of numerical experiments are conducted to test the impact of the NRT GVF datasets derived with the above two different methods and their relative performance in both offline Noah LSM simulations and WRF-ARW forecasts. As for the offline LSM, the benefit over a long-term period (13 years) is analyzed. Noah LSM simulations are performed from 2000 to 2012, using spectral- and biophysical-based GVF as inputs separately with identical meteorological forcing data. SM estimates from the Noah runs are then compared to the in situ measurements from the NASMD network to access their performance. As for the WRF Model, our study targets a 2-week period from 9 to 22 April 2015. The study period is of particular interest because of a significant drought event that occurred across much of the contiguous United States (CONUS). This case is able to serve as a good benchmark for assessing the impact of the proposed vegetation anomaly and its effect on land-atmosphere coupling. The semicoupled LIS-WRF runs are carried out using the spectral and biophysical GVF datasets separately while keeping the settings of the model grid, biophysical process schemes, and boundary conditions the same. More details of experiments settings for the offline Noah LSM and NWP model are given in the following sections.

##### 1) EXPERIMENT ON OFFLINE NOAH MODEL

In this experiment, the Noah simulation is set up over the CONUS (24°–50°N, 125°–65°W) at 0.125° spatial resolution, with the validation period of the growing season (April–October) from 2000 to 2012. The Noah model is integrated forward using a 30-min time step, forced by the NLDAS-2 forcing (Xia et al. 2012a,b). The Noah runs output daily SM fields (in volumetric soil moisture;  $\text{m}^3 \text{m}^{-3}$ ) for analysis, from which the first layer is used for surface SM analysis and the top three layers are weighted averaged to obtain root-zone SM. To create realistic initial variability in SM states, the Noah SM profile is uniformly initialized and spun up for a period from 1 January 1999 to 31 December 2012, and all the simulations are initialized at 1 January 1999 with the analysis field from spinup and rerun through 31 December 2012.

To demonstrate how the two GVF datasets impact the accuracy of the Noah SM estimates, Noah LSM simulations are performed using one GVF input at a time while other meteorological forcing parameters are unchanged. SM estimates from these two Noah LSM runs are then validated against in situ SM measurements

from the NASMD network over the CONUS. The differences in three statistical metrics (bias, root-mean-square error, and correlation) are examined to evaluate the relative performance of the two GVF datasets. The differences between these two datasets are tested for statistical significance at a confidence interval of 95%.

Along with the experiments using EVI- and LAI-based GVF, the Noah model runs with a default implementation of GVF climatology are carried out at the same time, serving as benchmark. The climatology GVF dataset used in the current NCEP operational Noah LSM is a 5-yr (1985–89) average derived from AVHRR observations. It provides a monthly specification of GVF with a spatial resolution of  $0.144^\circ$  in a latitude–longitude projection (Gutman and Ignatov 1998). Therefore, three experiments are carried out using 1) climatology GVF, 2) spectral-based GVF (EVI), and 3) biophysical-based GVF (LAI).

## 2) EXPERIMENTS ON WRF FORECAST MODEL

With the tools introduced in section 3a, a semicoupled LIS–WRF framework is designed to test how the two different GVF derivation methods affect WRF weather forecasts. In the coupling workflow, WRF provides atmospheric forcing data to LIS, and LIS sets up the simulation domain on the same grid (spatial resolution and projection) with the same terrestrial data and land surface physics (identical versions of the Noah LSM) as in the WRF run. The insertion of different GVF inputs is conducted within LIS. LIS then generates updated initializations and returns those updated initial land surface data (SM, soil temperature, fluxes, albedo, etc.) to WRF for next-day forecasts. Initializations of land states are updated based on the different GVF inputs, which will impact the subsequent forecasts in response to the changes in signals of surface vegetation cover.

Similar to the Noah offline run, the WRF run with the default implementation of GVF climatology is conducted as the reference. Therefore, three WRF experiments are carried out in this analysis using 1) climatology GVF (WRF-CLIM), 2) spectral-based GVF (WRF-EVI), and 3) biophysical-based GVF (WRF-LAI). The study domain is configured at 12-km spatial resolution in a Gaussian projection over North America. The LIS–WRF runs are conducted for 14 days from 9 to 22 April 2015. From 16 April, WRF forecasts for each time step (four steps a day for 7 days) are used to evaluate the impacts of the two GVF derivation approaches. Each model run is set up for 48-h forecasts, with hourly outputs starting from a fixed initialization time (0600 UTC). The 6-hourly GFS data are employed as forcing data to initialize the WRF-ARW model runs. The model configuration is summarized in detail in

**Table 1.** The settings of model grid, physical process schemes, and boundary conditions are kept the same for all three experiments.

## 4. Results and analysis

### a. GVF differences

#### 1) DIFFERENCE OF THE TWO GVF DERIVATION METHODS

The difference of the two GVF derivation methods can be analyzed by their responses to the same EVI variations. The spectral GVF is calculated from EVI with Eq. (1). Based on the results reported in Tanaka et al. (2015), a relationship between EVI and LAI for winter wheat is obtained as

$$\text{EVI} = 0.173 + 0.554(1 - e^{-0.656\text{LAI}}). \quad (3)$$

Inversing Eq. (3), the relationship between LAI and the EVI can be obtained as

$$\text{LAI} = -\ln[1 - (\text{EVI} - 0.173)/0.554]/0.656. \quad (4)$$

Combining Eqs. (2) and (4), the relationship between the EVI and the biophysical GVF can be plotted in Fig. 1.

From Fig. 1, the biophysical GVF could be significantly smaller than the spectral GVF for the same EVI observations. The spectral GVF values could become unrealistic when EVI is larger than  $\sim 0.6$ , indicating that EVI still has the saturation issue for dense vegetation canopy similar to NDVI (Huete et al. 2002).

#### 2) DATA PRODUCT DIFFERENCES

The global map of the GVF difference between the spectral- and biophysical-based GVF products is shown in the left panel of Fig. 2. The difference, averaged over a 10-yr period (2007–16), implies that these two GVF products vary significantly over space. The largest disagreement can reach over 20%. The spectral GVF is considerably lower over forest regions in general, such as the Amazon rain forests and tropical rain forests, while they are significantly higher over grassland and temperate broadleaf and mixed forests, especially over agricultural regions such as the U.S. Corn Belt, northern and northeastern China, and southern Europe. Zooming in for the CONUS domain (Fig. 2, right), the LAI-based biophysical GVF data are higher (negative difference) than the EVI-based GVF over forest regions such as the western and southeast coastal regions as well as the states of Louisiana, Mississippi, and Alabama. However, the spectral GVF data are significantly higher in the agricultural regions in the Midwest and southeastern



TABLE 1. LIS–WRF model configuration details.

Variables	Assignment
WRF dynamical core	WRF-ARW
Grid spacing	12 km
Dimension (west–east by south–north)	480 × 400
Integration time step	24 s (the same in LIS and WRF-ARW)
Vertical dimension	30
Number of soil levels or layers	4
Land usage	MODIS (20 category)
Microphysics	5 (Eta microphysics: the operational microphysics in NCEP models)
Land surface	Noah (v3.3)
Planetary boundary layer	Mellor–Yamada–Janjić scheme

Texas by over 20%, and moderate in the Great Plains region on the order of 5%–10%, compared to the biophysical GVF data product, which is consistent with the results shown in Fig. 1. The variation over the western desert region is mixed and relatively small, with a difference of less than 5%.

An agricultural-based site at Bondville, Illinois (40.178°N, 88.771°W) is selected to show how much the biophysical-based GVF data differ from spectral-based data over time. The dynamics of GVF based on EVI and LAI methods at Bondville over the warm season in 2008 are shown in Fig. 3. The plot shows significant differences between these two GVF datasets in terms of the range and the rate of change. The GVF dataset derived from EVI suffers perceived defects from the spectral-based remotely sensed VIs, which confirms the unrealistic GVF values associated with high EVI in Fig. 1. The dynamic of the spectral-based GVF exhibits an obvious saturation when the vegetation grows beyond a certain threshold, which leads to losing the sensitivity to vegetation growth throughout the period from late summer to early fall. The changes during green-up and senescence phases estimated from the EVI-based GVF are at a much faster rate than those from the LAI-based one. The EVI-based GVF reaches a value of 1 in mid-July and remains at the status of full vegetation cover for nearly 2 months before a sharp decrease starting in mid-September. The biophysical-based GVF, on the other hand, exhibits continuous growth of vegetation cover by about 20% from mid-July to mid-August and a gradual decrease afterward. The GVF changes reflected in the LAI-based dataset are more representative of the actual condition of the vegetation cover and yet are completely missed in the EVI-based GVF dataset because of its saturation issue. The use of a more accurate GVF input into LSMs would definitely reduce the uncertainties in

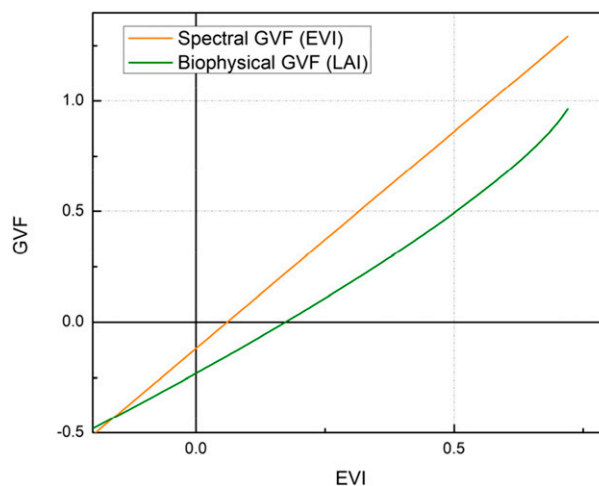


FIG. 1. The relationship between the spectral GVF (orange line) or the biophysical GVF (blue curve) and the EVI for winter wheat [based on results in Tanaka et al. (2015)].

the mode initialization, which in turn could improve the model's capability of simulating land surface states.

#### b. Evaluation of the Noah offline simulations

##### 1) IMPACT OF GVF DIFFERENCES ON NOAH MODEL SIMULATIONS

The significant variation in GVF inputs into the Noah LSM is expected to notably impact the surface energy budget in model simulations. Differences in heat flux estimates (sensible, latent, and ground flux components) from the Noah LSM over the Northern Mountain region (40°–49.4°N, 118°–104°W) and Oklahoma–lower Mississippi region (29.8°–39.2°N, 103°–88°W) are shown in Fig. 4, along with regional GVF difference maps as a reference. The mean difference map averaged over validation period (9–22 April 2015) demonstrates significant impact on both regions. The patterns of flux difference match well with that of input GVF difference where higher GVF inputs lead to a rise in latent heat flux and a drop in sensible flux simulations and vice versa. Estimates of sensible heat fluxes from the Noah run with EVI-based GVF have seen an overall decrease by about  $22 \text{ W m}^{-2}$  in Oklahoma, and yet a substantial rise in Louisiana and southern Arkansas on the order of  $20\text{--}50 \text{ W m}^{-2}$ . Simulations of latent heat fluxes, on the other hand, are regionally altered on the same level in terms of magnitude but in the opposite trend.

The water balance is also inevitably altered by changes in surface GVF inputs. The impact is expected to be significant on both surface and root-zone estimates from the long-term run. The normalized difference of surface (left) and root-zone SM (right) estimates from the Noah LSM caused by the variation in these two

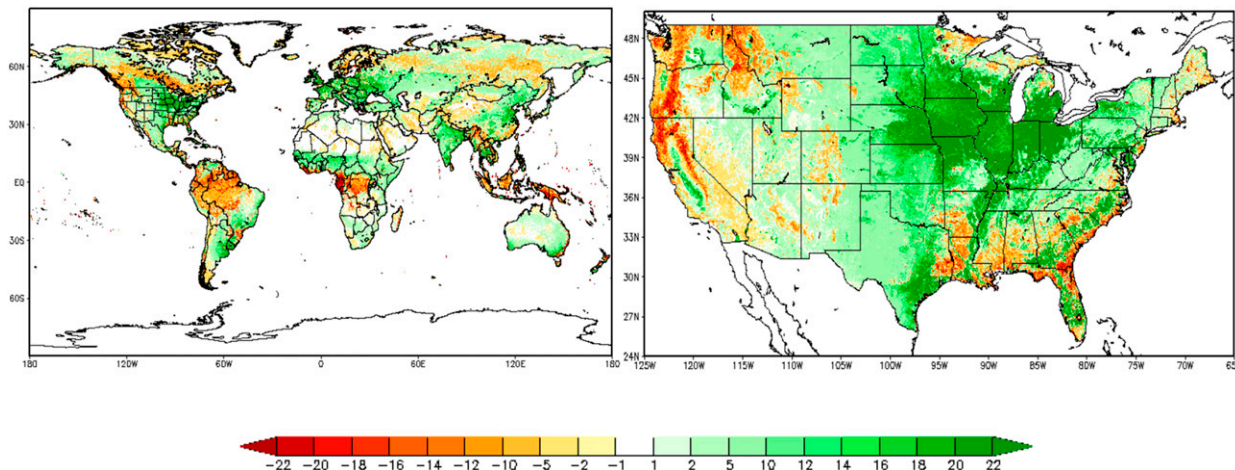


FIG. 2. GVF differences between EVI- and LAI-based GVF products (GVF\_EVI minus GVF\_LAI) (left) over the global domain and (right) over the CONUS domain, averaged over the period of 2007–16.

different GVF inputs are shown in Fig. 5. The long-term average difference is on the 10-yr basis from 2007 to 2016. The patterns of differences in surface and root-zone SM estimates are similar but the influence to root-zone SM estimates is considerably larger by around 15%. The impact over the western United States appears to be much larger than that over the east under both dry and wet conditions.

Notably, the sensitivity of the Noah LSM to GVF input is dependent on land surface type. For instance, about 18%–20% of GVF variation leads to a 5% difference in surface SM estimates and up to 16% in the root zone in Nebraska, while the impact at the same level of GVF variation is very limited on the eastern coast. The histogram of the normalized SM differences (both surface and root zone; normalized by multiple-year mean SM) as the

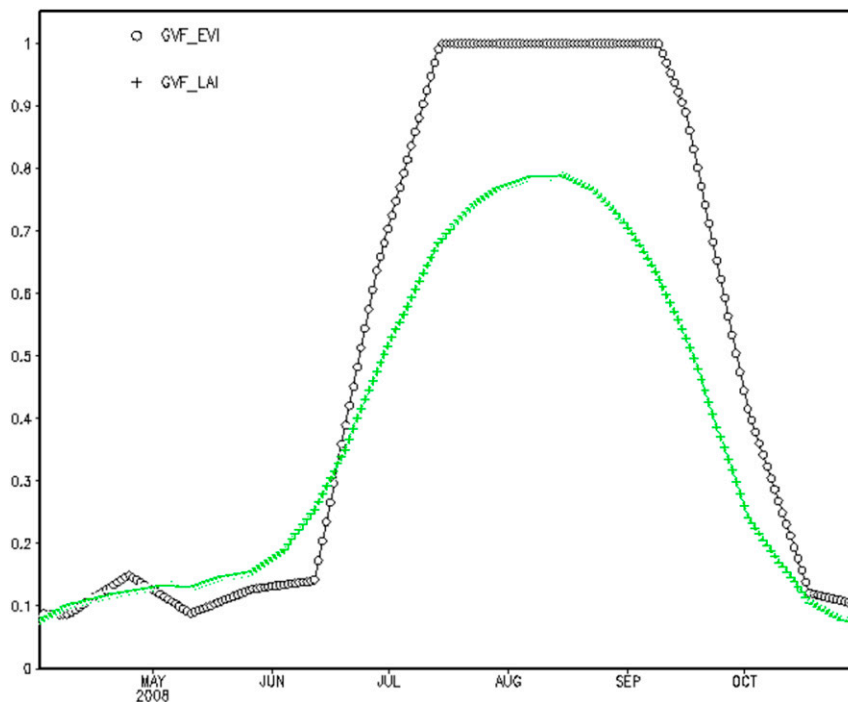


FIG. 3. GVFs converted from EVI and LAI over the growing season in 2008 at Bondville, Illinois (40.178°N, 88.771°W).

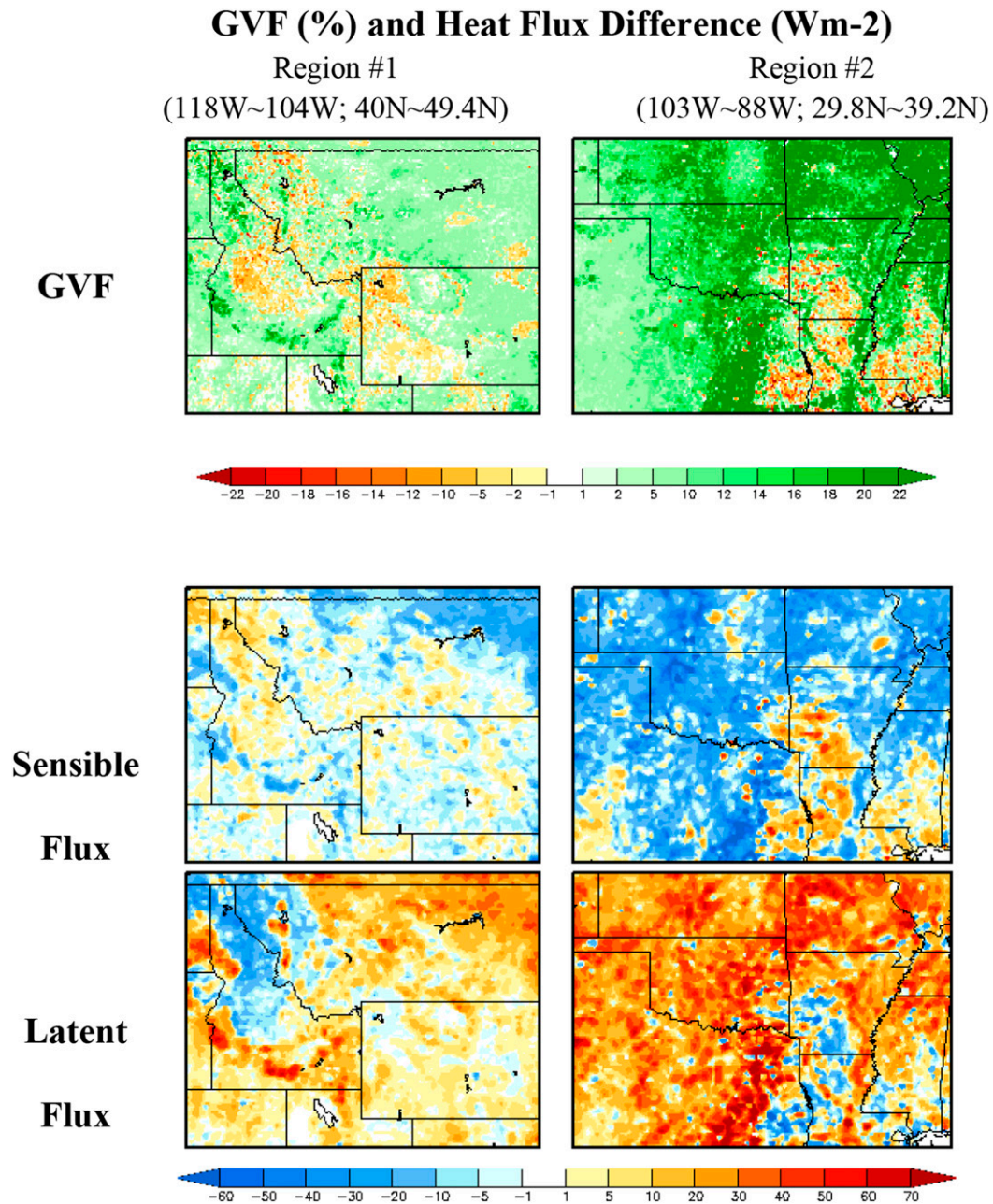


FIG. 4. GVF difference and corresponding changes of heat flux estimations from the Noah model (Noah run with EVI-based GVF minus the LAI-based one) between 9 and 22 Apr 2015 over two regions: 118°–104°W, 40°–49.4°N and 103°–88°W, 29.8°–39.2°N.

function of land surface type is shown in Fig. 6. The mean differences of normalized GVF over each land type are also shown in the figure as a reference. It is interesting to notice that the Noah LSM is more sensitive to the GVF change over shrubland, grassland, and cropland. Taking the cropland as an example, around 3% of surface SM estimates and as high as 5.5% at the root zone can be detected corresponding to the surface GVF variation.

However, the impact on Noah SM estimates over deciduous broadleaf forest is within 1% for both the surface and root zone.

## 2) EVALUATION OF THE NOAH OFFLINE SM SIMULATIONS

The Noah offline SM estimates are validated against the ground observations from the NASMD network.



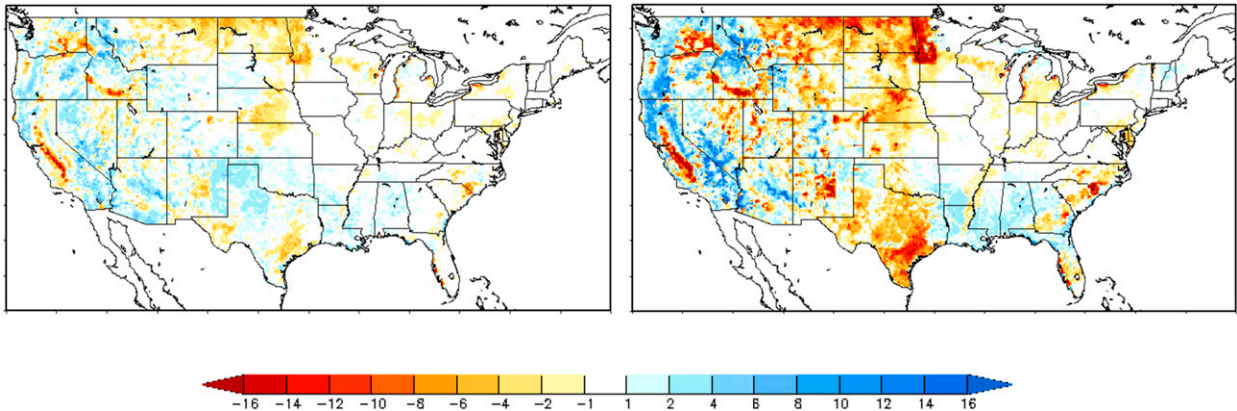


FIG. 5. Normalized changes of (left) surface and (right) root-zone SM estimates from the Noah LSM when two different GVF inputs are introduced in the Noah model over the warm season (April–October) between 2007 and 2016.

The root-mean-square error (RMSE) and correlation of surface soil moisture estimates from three Noah simulations (with climatology and spectral- and biophysical-based GVF inputs) are shown in Fig. 7. Verification results generally show the insertion of near-real-time GVF, either spectrally or biophysically based, is beneficial to improving model soil moisture simulations with decreased RMSE and enhanced correlation compared to the runs using GVF climatology. Larger impacts can be found between day of year (DOY) 127 and 157, as well as for DOY 223–289.

To better illustrate relative performances of the two NRT GVF datasets, the relative differences (RDs) between Noah runs with EVI- and LAI-based GVF are then computed and compared. First, the bias, RMSEs, and correlations of surface and root-zone SM estimates are computed separately for Noah model runs with

spectral and biophysical GVF as inputs. Second, the RD of bias and RMSE is calculated as  $(RD_{Noah\_EVI} - RD_{Noah\_LAI})/RD_{Noah\_EVI}$ , while the RD of the correlation is computed as  $(RD_{Noah\_LAI} - RD_{Noah\_EVI})/RD_{Noah\_EVI}$ . The positive values represent SM estimates from the Noah LSM using LAI-based GVF that have smaller errors or higher correlation compared to the in situ SM observations from NASMD, meaning the use of biophysical-based GVF improves the accuracy of the Noah SM estimates. Again, the differences are tested for statistical significance at a confidence interval of 95%. The RD of bias, RMSE, and correlation on each DOY over the warm season is shown in Fig. 8. The validation results reveal that the biophysical-based GVF outperforms the spectral-based GVF dataset in general for both surface and root-zone SM estimates. It can be further concluded that the improvement in root-zone

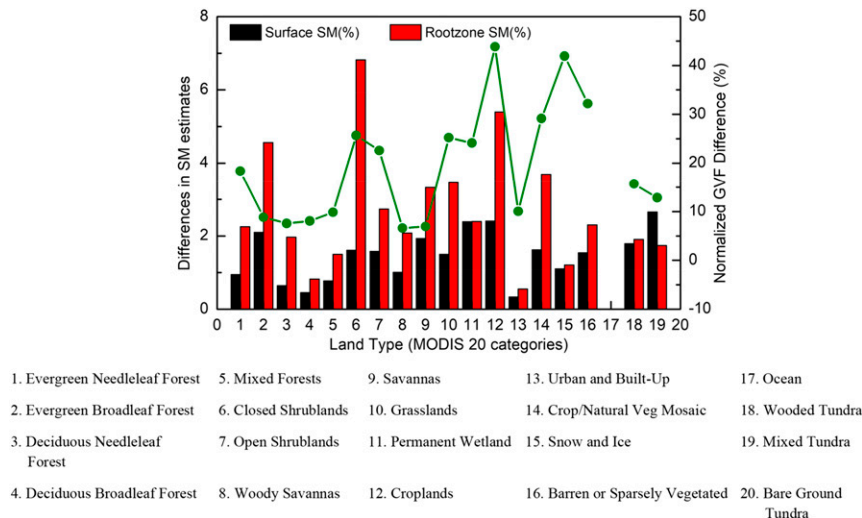


FIG. 6. Differences in normalized SM estimates over different land types.

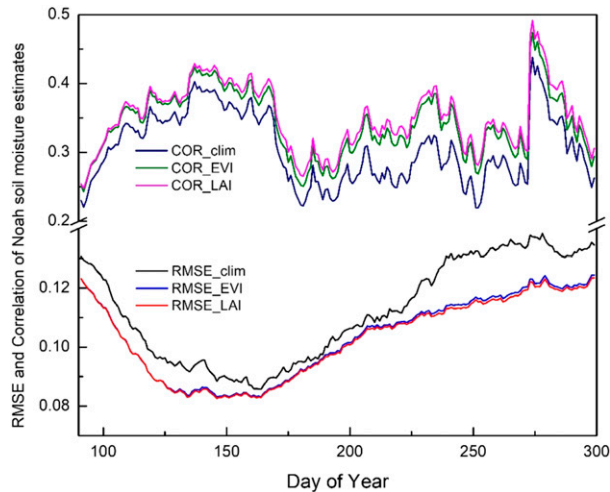


FIG. 7. RMSE ( $\text{m}^3 \text{m}^{-3}$ ) and correlation of Noah SM estimations validated against in situ measurements for the warm season (April–October) averaged over the CONUS domain.

SM estimates when using GVF converted from LAI is significantly larger than that in surface SM by 1.2% in bias, 4.2% in RMSE, and 17.7% in correlation.

At the early stage of the warm season, the precision of Noah SM estimates with the LAI-based GVF is slightly higher than that with the EVI-based input. The differences between the two GVF datasets steadily drop down from spring to early summer, which indicates both GVF datasets are equally capable of capturing vegetation green-up trends from May to June. However, at the turning point of early July, the use of biophysical-based GVF becomes more beneficial to the Noah SM estimates, and the positive impact steadily increases from July to October. It is understandable and reasonable when taking a look at Fig. 8 and Fig. 3 in parallel. During the period from July to October, the land vegetation information interpreted from EVI is always at full coverage, while LAI-based GVF provides additional dynamic information of an increasing trend from July to August, followed by a decrease starting in September. In the Noah LSM, the proportion of the three components of evaporation is very sensitive to the GVF parameter (Gutman and Ignatov 1998), and thus the surface energy balance can be largely changed responding to the change in GVF. In other words, the accurate representation of green vegetation cover is crucial to the Noah LSM to estimate flux components correctly, which further determines the accuracy of predictions in land surface variables such as soil moisture. The increase of GVF from July to August and the decrease in September by about 20% in each phase is absolutely critical information to the Noah model to partition total evapotranspiration in a more accurate way. The validation results clearly

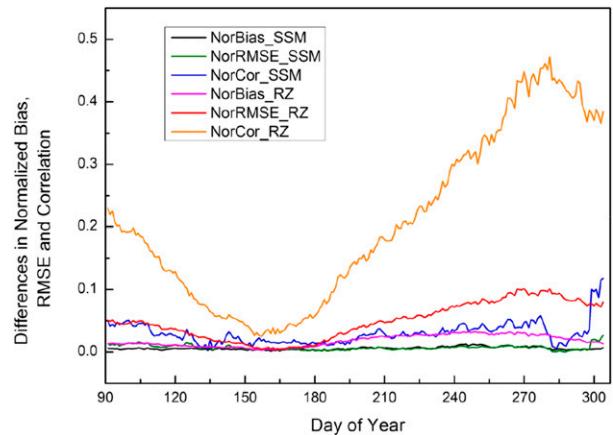


FIG. 8. RDs of bias, RMSE, and correlation between Noah SM estimates using spectral- and biophysical-based GVF datasets with respect to in situ observations on each DOY over the growing season (April–October), averaged from 2007 to 2016.

demonstrate the added skill of LAI-based GVF, particularly over the period of July and October. Overall, the use of GVF converted from LAI improves the accuracy of Noah SM estimates over 65.3% of the NASMD sites for the surface and over 66.2% for root zone.

Moreover, the average differences in error statistics for root-zone SM estimates are calculated as a function of GVF variation at a 5% interval. The frequency histogram is shown in Fig. 9. Noah root-zone SM estimates with biophysical-based GVF input present overall less bias and RMSE and higher correlation with respect to the ground validation dataset, except for slightly larger bias and RMSE when the GVF variation is at the level of 10%. The larger the variation that the two GVF datasets have, the higher the positive impact of the Noah model responses to biophysical GVF input. The improvement in root-zone SM estimates by using LAI-based GVF is 1.0% in bias and 3.2% in correlation on average when GVF variation is less than 30%, while the improvement increases to an average of 6.2% in bias and 8.9% in correlation when the GVF variation reaches 30% and larger. The mean improvement in normalized bias, RMSE, and correlation at all levels of GVF differences combined are 4.7%, 1.7%, and 6.7%, respectively.

### 3) EVALUATION OF THE NOAH OFFLINE FLUX SIMULATIONS

This section will present results on verification of soil heat conduction flux  $G$  and sensible  $H$  and latent  $\lambda \text{ET}$  flux estimates from the Noah LSM using different GVF sources. Given that the land surface models and weather forecast models in our experiment operate on a regional scale at coarse spatial resolution ( $\sim 12 \text{ km}$  in our experiment), verification using the footprint of surface flux

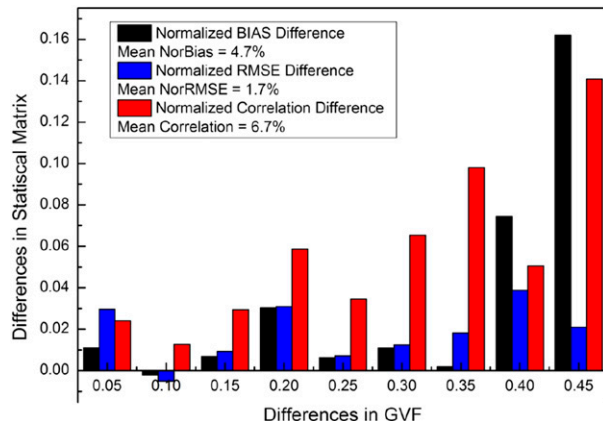


FIG. 9. Frequency histogram of relative differences of bias (black), RMSE (blue), and correlation (red) as a function of GVF variation.

observations occurring on a scale of 0.1–1 km is often hampered by a scale mismatch issue (Anderson et al. 2004, 2011; Doran et al. 1998; Gao et al. 1998). The limitation of direct comparison with tower flux observations is further exacerbated over heterogeneous land cover pixels, where one surface flux tower location may not have vegetation properties that are representative of the complete 12-km pixel. In our study, instead of using tower flux observations, the Atmosphere–Land Exchange Inverse (ALEXI) model is selected to evaluate the relative performance of the land surface model with different GVF datasets considering that 1) the ALEXI model has demonstrated satisfactory reliability of its ET estimates, 2) the ALEXI model is able to provide accurate partitioning of sensible and latent heat fluxes across the CONUS (Anderson et al. 2007, 2011), and 3) the ALEXI model operates at comparable spatial resolution as in our experiments. Therefore, ALEXI model simulations are assumed to serve as a good reference for the ET evaluation effort.

The ALEXI model is built on the two-source energy budget (TSEB) approach of Norman et al. (1995), which partitions the composite surface radiometric temperature into characteristic soil and canopy temperatures, based on the fraction of vegetation cover. In ALEXI, the lower boundary conditions for the two-source model are provided by thermal infrared observations taken at two times during the morning hours from GOES. For regional applications, the TSEB model has been coupled with a one-dimensional atmospheric boundary layer (ABL) model (McNaughton and Spriggs 1986). The ABL model then relates the rise in air temperature above the canopy during this interval and the growth of the ABL to the time-integrated influx of sensible heating from the surface, and ET is computed as a partial residual to the energy budget.

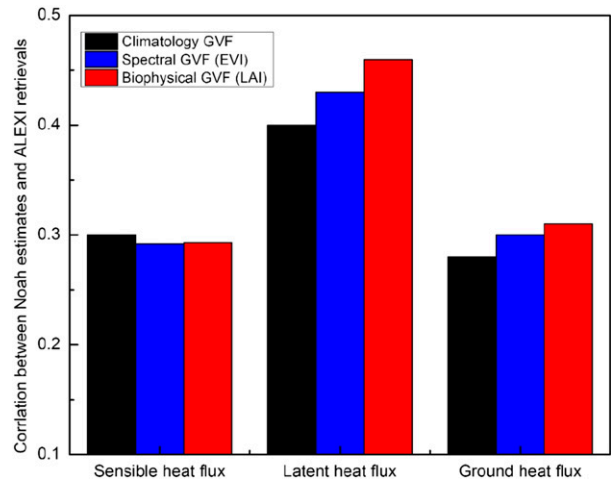


FIG. 10. Noah flux estimates (sensible, latent, and ground heat fluxes) validated against ALEXI flux component retrievals, showing comparison among the Noah LSM runs with climatology and spectral and biophysical GVF datasets.

The time series of correlation of the sensible, latent, and ground flux components between ALEXI retrievals and Noah simulations are shown in Fig. 10. Better agreements of the Noah model latent and ground heat flux simulations with the ALEXI model retrievals are obtained when either spectral or biophysical GVF has been used. However, sensible heat flux simulations from Noah show a slight degradation using near-real-time GVF compared to GVF climatology. Notably, Noah ET estimates using LAI-based GVF presents the best agreement with ALEXI retrievals.

In addition, Noah estimates of the Bowen ratio are compared with ALEXI retrievals to evaluate the relative value of near-real-time spectral- and biophysical-based GVF datasets to the Noah model from another perspective (Fig. 11). The same conclusion can be drawn from the Bowen ratio comparison that biophysical-based GVF is more beneficial to surface energy flux simulations for the Noah land surface model.

### c. Evaluation of WRF forecasts using different GVF inputs

After evaluating how spectral and biophysical GVFs impact offline Noah runs, this section focuses on the assessment of WRF forecasts using ground weather observations from over a thousand ground sites. A sensitivity analysis is given first, followed by the quantitative validation.

#### 1) IMPACT OF GVF DIFFERENCES ON WRF FORECASTS

The comparison of WRF 2-m surface temperature (T2m) forecasts at 1800 UTC between WRF runs using

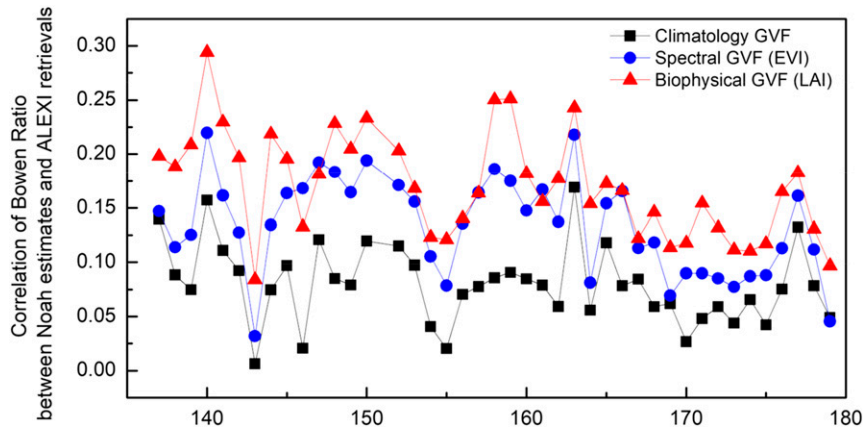


FIG. 11. Correlation of the Bowen ratio between Noah estimates and ALEXI retrievals, showing comparison among the Noah LSM runs with climatology and spectral and biophysical GVF datasets.

GVF climatology and NRT GVF (EVI and LAI based) is shown in Figs. 12a and 12b for WRF\_EVI run minus WRF\_CLIM and WRF\_LAI run minus WRF\_CLIM, respectively. The differences are averaged over a 1-week period from 16 to 22 April 2015. Compared with T2m forecasts using GVF climatology, both NRT GVFs predict warmer temperatures over the western United States and cooler forecasts over the northern East Coast as well as the boundary between Texas and Mexico. While utilization of EVI-based GVF does not show significant impact over the Midwest region, the replacement of LAI-based GVF remarkably increases forecasts of surface temperature compared to WRF\_CLIM run.

When intercomparing T2m forecasts between WRF runs with these two NRT GVF inputs (Fig. 13, left), T2m forecasts are generally lower from WRF runs with EVI-based GVF on the order of 0.4–2.6 K over the majority of the central and eastern United States, yet significantly

higher in southern Nevada and the southern West Coast. Similarly, the difference in 2-m relative humidity (RH2m) forecasts at 1800 UTC is shown in Fig. 13 on the right. In general, the pattern of RH2m variation matches well with that of T2m but with the opposite trend. The patterns are physically sound as T2m drops in the WRF run using EVI-based GVF over most of the central and eastern regions in response to a positive anomaly compared to LAI-based GVF, which in turn increases surface humidity, and vice versa in other areas.

## 2) EVALUATION OF WRF FORECASTS

To quantitatively analyze which GVF derivation method performs better when introduced in WRF, forecasts from the three WRF runs (T2m and RH2m) using climatology GVF and EVI- and LAI-based GVF are evaluated against ground weather observations from nearly a thousand ground sites.

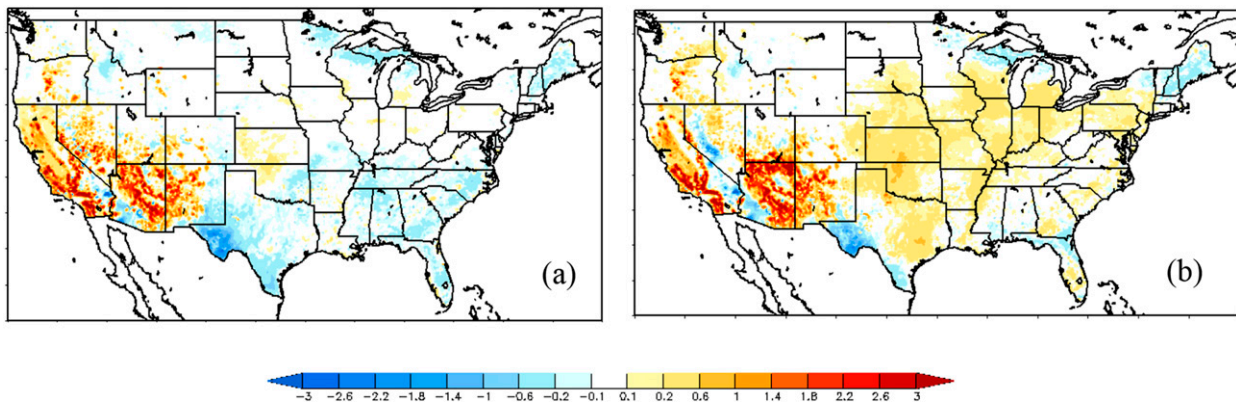


FIG. 12. Difference in WRF T2m at 1800 UTC, averaged over the period of 16–22 Apr 2015 for (a) WRF\_EVI run minus WRF\_CLIM and (b) WRF\_LAI run minus WRF\_CLIM.



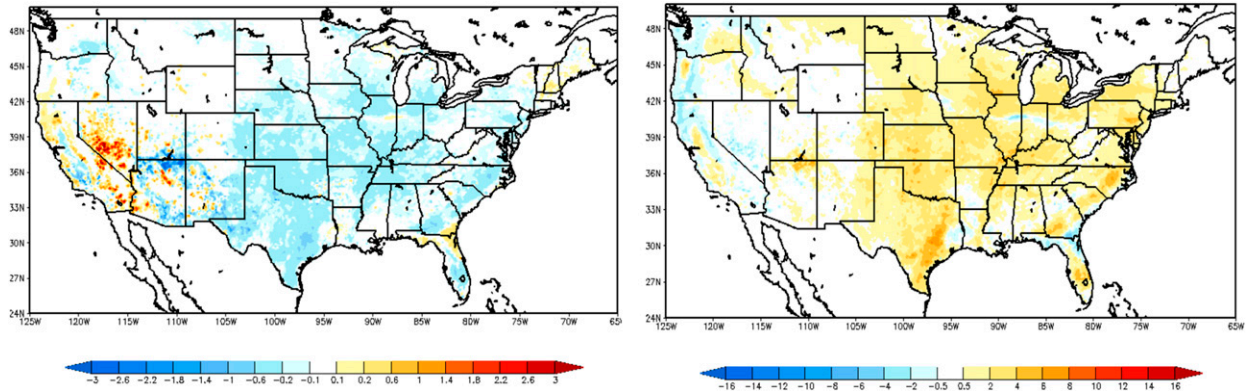


FIG. 13. Difference in (left) T2m and (right) RH2m at 1800 UTC between WRF runs using spectral- and biophysical-based GVF (WRF\_EVI run minus WRF\_LAI run), averaged over the period of 16–22 Apr 2015.

Time series comparison of T2m (solid lines) and RH2m (dashed lines) at 1800 UTC between WRF forecasts and in situ observations (green dot–dashed lines) from 16 to 23 April 2015 is shown in Fig. 14 for day 1 forecasts on the left and day 2 on the right. At this sample site in California (37.37°N, 118.37°W), the area is under a drought, and therefore it is obvious that the WRF run using climatology GVF predicts significant lower T2m and higher RH2m during daytime because of the overestimation of surface green cover over that period. The use of NRT GVF inputs (either spectral or biophysical based) is able to reduce the bias in both T2m and RH2m to a great extent. Worth noting is that the biophysical LAI-based GVF shows more benefits to the bias reduction than the spectral EVI-based one (red lines versus blue lines). The positive impact of biophysical LAI-based GVF is consistently detected for

both day 1 and day 2 WRF forecasts by removing the cold bias in T2m, while using EVI-based GVF presents a slight degradation in day 2 forecasts.

Taking an overall review of validation results from about 840 ground sites over the CONUS domain, RMSEs of those three WRF forecasts at 1800 UTC on each day of the validation period (16–22 April 2015) are compared for T2m (top) and RH2m (bottom) and for day 1 (left) and day 2 (right) separately as shown in Fig. 15. Both T2m and RH2m forecasts using GVF climatology depict highest uncertainty in general, with RMSE in T2m (RH2m) on the order of 1.9–2.4 K (9.0%–10.0%) for day 1 forecasts. The accuracy of WRF T2m forecasts with insertion of EVI-based GVF are overall improved, with a slight degradation on 22 April for day 1 forecasts as well as 21 and 23 April for day 2. On the other hand, RMSEs of T2m forecasts remarkably drop with the introduction of biophysical GVF

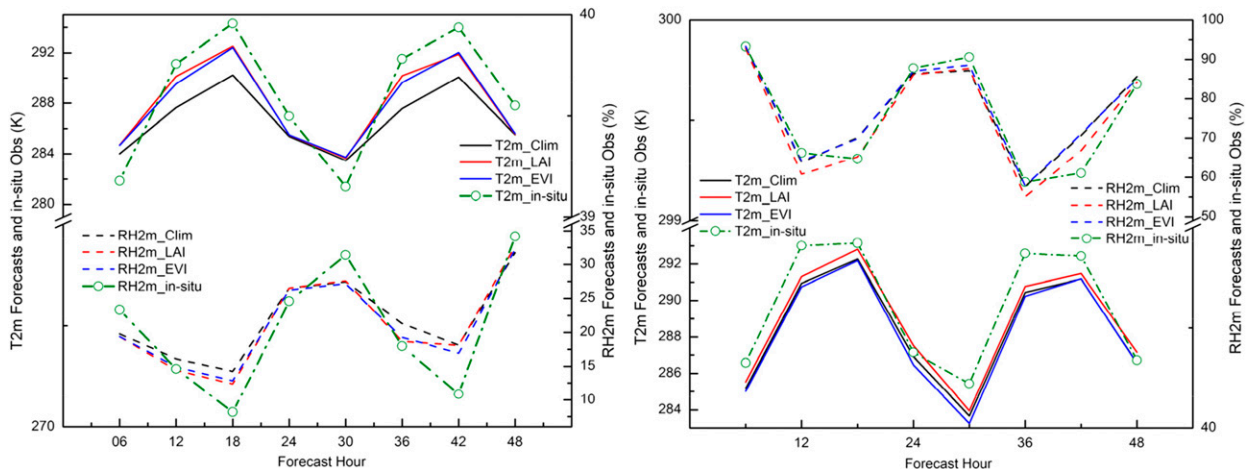


FIG. 14. Comparison of time series of T2m (solid lines) and RH2m (dashed lines) between WRF forecasts and in situ observations (green dot–dashed lines) in California (37.37°N, 118.37°W) at 1800 UTC, averaged over the period of 16–22 Apr 2015, for (left) day 1 and (right) day 2 forecasts.

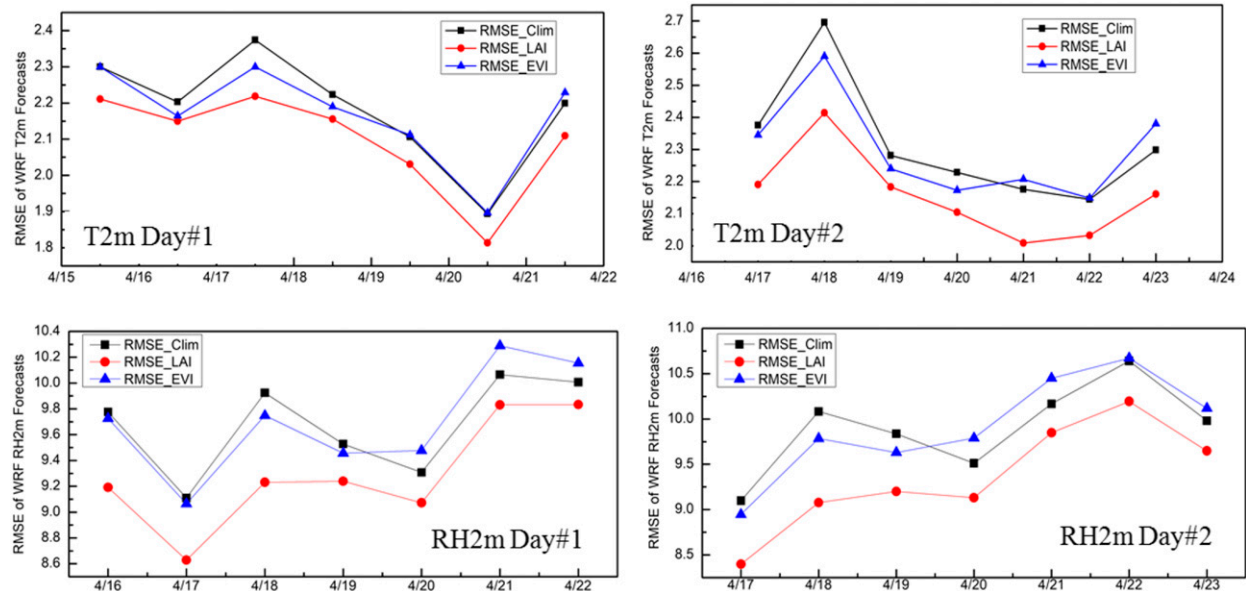


FIG. 15. Validation of (top) T2m and (bottom) RH2m forecasts from WRF runs using  $\sim 840$  ground sites over the CONUS; RMSEs of WRF runs using climatology (black) and EVI-based (blue) and LAI-based (red) GVF at 1800 UTC 16–22 Apr 2015, for (left) day 1 and (right) day 2 forecasts.

by nearly 0.1 for day 1 and 0.16 for day 2 forecasts on average. As for the validation on RH2m forecasts, using EVI-based GVF provides certain added value before 20 April but not for the rest of the week. On the contrary, the use of LAI-based GVF significantly reduces RMSE for both days. The improvements brought by the biophysical GVF are more consistent and at a larger magnitude compared to spectral GVF.

Difference maps in RMSEs for each of the validation sites are capable of presenting improvement/degradation from a spatial perspective. The differences over each site are tested for statistical significance with a significance level of 0.05. As shown in Fig. 16, the RMSE difference is computed by the WRF–EVI run minus WRF–LAI runs over  $\sim 840$  ground sites collected from the Global Upper Air and Surface Weather Observations, with positive (negative) values meaning that forecasts from the WRF–EVI run show larger (smaller) error than those using LAI-based GVF. The sites with warm (cool) colors shown in the map are where biophysical LAI-based GVF outperforms (underperforms) the spectral EVI-based one. Evidently, for T2m forecasts, the WRF Model performs better with LAI-based GVF input over the majority of the sites across the country, with an exception over Iowa and parts of North Dakota. Moreover, LAI-based GVF has compelling advantages in improving WRF RH2m forecasts compared to the spectral-based GVF.

## 5. Summary and discussion

Better representation of GVF is crucial to LSMs for precisely describing current vegetation states, which can improve the accuracy of the partitioning of surface sensible and latent heat fluxes (Kurkowski et al. 2003). As the weakness of spectral-based GVF (converted from NDVI or EVI) is recognized, this paper proposes to create a biophysical GVF product from LAI, which is an intrinsic physical quantity. We first quantify their differences and then analyze their impacts on an offline LSM and coupled weather forecast model. The comparison revealed huge variations between spectral- and biophysical-based GVF datasets from both spatial and temporal aspects. The significant differences within these two GVF datasets inevitably affect the accuracy of predictions from the Noah LSM and weather forecast models.

Simulations from uncoupled Noah LSM and forecasts from the WRF Model are obtained using either spectral or biophysical GVF inputs while meteorological forcing and other settings were kept the same. The soil moisture simulations from the offline Noah runs and the weather forecasts from WRF runs were then evaluated using in situ measurements or reanalysis products to assess their performance.

As for offline Noah simulations, the surface and root-zone SM estimates are validated against in situ SM measurements from NASMD over the period from 2000 to 2012. Validation results show that the

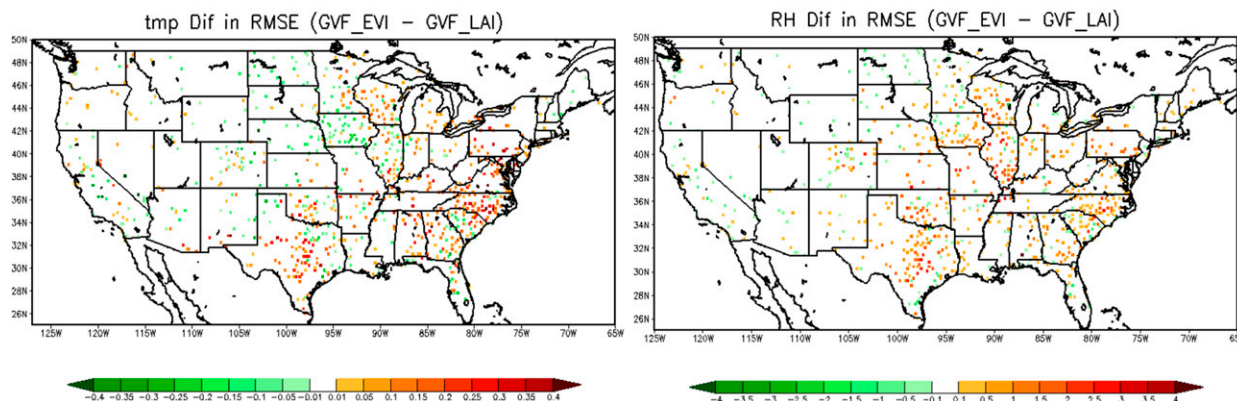


FIG. 16. Difference in RMSE of (left) T2m and (right) RH2m forecasts between WRF run with EVI-based and LAI-based GVF during the daytime, WRF-EVI run minus WRF-LAI run; warm (cool) color means added (degraded) value.

biophysical-based GVF outperforms the spectral-based one in general, and the positive impact on root-zone SM estimates is significantly larger than that on surface SM. The use of GVF converted from LAI improves the accuracy of Noah SM estimates over 65.3% of the NASMD sites for the surface and over 66.2% for the root zone. It is even more promising to see that using LAI-based GVF particularly outperformed the spectral-based one over the period of July–October when the biophysical GVF is able to provide an additional vegetation dynamic while the spectral one suffers from the saturation issue.

This study further assessed the impact of two different GVF datasets on coupled atmospheric prediction models. Once again, significant variation is found in near-surface predictions from WRF when using those two different GVF derivation methods. The WRF Model predicted lower 2-m surface temperature and higher surface humidity using spectral-based GVF over vast parts of the central and eastern regions than it did using the biophysical-based GVF. Evaluation of T2m and RH2m forecasts from the WRF Model shows the use of biophysical GVF is capable of consistently improving the accuracy of WRF T2m and RH2m forecasts for both days, compared to that of spectral GVF.

In conclusion, our preliminary evaluation results show the accuracy of NCEP Noah LSM soil moisture estimates and WRF Model forecasts increases when using biophysical-based GVF with improved sensitivity in high-biomass regions. With the increasing need for the accurate representation of green vegetation status in land surface models, both spatially and temporally, attempts to create a better remotely sensed GVF dataset are worth further research.

*Acknowledgments.* This work was supported by three funding sources, which are the NOAA NESDIS GOES-R

Risk Reduction Program (GOES-R3); NOAA NESDIS JPSS Proving Ground and Risk Reduction Program (JPSS PGRR); and NOAA Climate Program Office Modeling, Analysis, Prediction and Projections (MAPP) program. The authors would also like to thank Gao Feng for help on providing smoothed and gap-filled MODIS LAI software package.

#### REFERENCES

- Abramopoulos, F., 1988: Generalized energy and potential entrophy conserving finite-difference schemes for the shallow-water equations. *Mon. Wea. Rev.*, **116**, 650–662, [https://doi.org/10.1175/1520-0493\(1988\)116<0650:GEAPEC>2.0.CO;2](https://doi.org/10.1175/1520-0493(1988)116<0650:GEAPEC>2.0.CO;2).
- Anderson, M. C., J. M. Norman, J. R. Mecikalski, R. D. Torn, W. P. Kustas, and J. B. Basara, 2004: A multiscale remote sensing model for disaggregating regional fluxes to micrometeorological scales. *J. Hydrometeorol.*, **5**, 343–363, [https://doi.org/10.1175/1525-7541\(2004\)005<0343:AMRSMF>2.0.CO;2](https://doi.org/10.1175/1525-7541(2004)005<0343:AMRSMF>2.0.CO;2).
- , J. M. Norman, W. P. Kustas, F. Li, J. H. Prueger, and J. R. Mecikalski, 2007: A climatological study of evapotranspiration and moisture stress across the continental United States: 1. Model formulation. *J. Geophys. Res.*, **112**, D10117, <https://doi.org/10.1029/2006JD007506>.
- , C. R. Hain, B. Wardlow, A. Pimstein, J. R. Mecikalski, and W. P. Kustas, 2011: Evaluation of drought indices based on thermal remote sensing of evapotranspiration over the continental United States. *J. Climate*, **24**, 2025–2044, <https://doi.org/10.1175/2010JCLI3812.1>.
- Bégué, A., 1993: Leaf area index, intercepted photosynthetically active radiation, and spectral vegetation indices: A sensitivity analysis for regular-clumped canopies. *Remote Sens. Environ.*, **46**, 45–59, [https://doi.org/10.1016/0034-4257\(93\)90031-R](https://doi.org/10.1016/0034-4257(93)90031-R).
- Carlson, T. N., and D. A. Ripley, 1997: On the relation between NDVI, fractional vegetation cover, and leaf area index. *Remote Sens. Environ.*, **62**, 241–252, [https://doi.org/10.1016/S0034-4257\(97\)00104-1](https://doi.org/10.1016/S0034-4257(97)00104-1).
- Case, J. L., F. J. LaFontaine, G. J. Jedlovec, S. V. Kumar, and C. D. Peters-Lidard, 2014: A real-time MODIS vegetation product for land surface and numerical weather prediction models. *IEEE Trans. Geosci. Remote Sens.*, **52**, 1772–1786, <https://doi.org/10.1109/TGRS.2013.2255059>.



- Chen, F., and J. Dudhia, 2001: Coupling an advanced land surface–hydrology model with the Penn State–NCAR MM5 modeling system. Part I: Model description and sensitivity. *Mon. Wea. Rev.*, **129**, 569–585, [https://doi.org/10.1175/1520-0493\(2001\)129<0569:CAALSH>2.0.CO;2](https://doi.org/10.1175/1520-0493(2001)129<0569:CAALSH>2.0.CO;2).
- , and Coauthors, 1996: Modeling of land surface evaporation by four schemes and comparison with FIFE observations. *J. Geophys. Res.*, **101**, 7251–7268, <https://doi.org/10.1029/95JD02165>.
- Doran, J. C., J. M. Hubbe, J. C. Liljigren, W. J. Shaw, G. J. Collatz, D. R. Cook, and R. L. Hart, 1998: A technique for determining the spatial and temporal distributions of surface fluxes of heat and moisture over the Southern Great Plains Cloud and Radiation Testbed. *J. Geophys. Res.*, **103**, 6109–6121, <https://doi.org/10.1029/97JD03427>.
- Ek, M. B., K. E. Mitchell, Y. Lin, E. Rogers, P. Grummann, V. Koren, G. Gayno, and J. D. Tarpley, 2003: Implementation of Noah land surface model advances in the National Centers for Environmental Prediction operational mesoscale Eta model. *J. Geophys. Res.*, **108**, 8851, <https://doi.org/10.1029/2002JD003296>.
- Gao, W., R. L. Coulter, B. M. Lesht, J. Qiu, and M. L. Wesely, 1998: Estimating clear-sky regional surface fluxes in the Southern Great Plains Atmospheric Radiation Measurement site with ground measurements and satellite observations. *J. Appl. Meteor.*, **37**, 5–22, [https://doi.org/10.1175/1520-0450\(1998\)037<0005:ECSRFS>2.0.CO;2](https://doi.org/10.1175/1520-0450(1998)037<0005:ECSRFS>2.0.CO;2).
- Gao, X., A. R. Huete, W. Ni, and T. Miura, 2000: Optical–biophysical relationships of vegetation spectra without background contamination. *Remote Sens. Environ.*, **74**, 609–620, [https://doi.org/10.1016/S0034-4257\(00\)00150-4](https://doi.org/10.1016/S0034-4257(00)00150-4).
- Gutman, G., and A. Ignatov, 1998: The derivation of the green vegetation fraction from NOAA/AVHRR data for use in numerical weather prediction models. *Int. J. Remote Sens.*, **19**, 1533–1543, <https://doi.org/10.1080/014311698215333>.
- Huete, A., C. Justice, and W. van Leeuwen, 1999: MODIS Vegetation Index (MOD13). Algorithm Theoretical Basis Doc., Version 3, 129 pp., [https://modis.gsfc.nasa.gov/data/atbd/atbd\\_mod13.pdf](https://modis.gsfc.nasa.gov/data/atbd/atbd_mod13.pdf).
- , K. Didan, T. Miura, E. P. Rodriguez, X. Gao, and L. G. Ferreira, 2002: Overview of the radiometric and biophysical performance of the MODIS vegetation indices. *Remote Sens. Environ.*, **83**, 195–213, [https://doi.org/10.1016/S0034-4257\(02\)00096-2](https://doi.org/10.1016/S0034-4257(02)00096-2).
- James, K. A., D. J. Stensrud, and N. Yussouf, 2009: Value of real-time vegetation fraction to forecasts of severe convection in high-resolution models. *Wea. Forecasting*, **24**, 187–210, <https://doi.org/10.1175/2008WAF2007097.1>.
- Jiang, L., and Coauthors, 2010: Real-time weekly global green vegetation fraction derived from advanced very high resolution radiometer-based NOAA operational global vegetation index (GVI) system. *J. Geophys. Res.*, **115**, D11114, <https://doi.org/10.1029/2009JD013204>.
- Jönsson, P., and L. Eklundh, 2002: Seasonality extraction by function fitting to time-series of satellite sensor data. *IEEE Trans. Geosci. Remote Sens.*, **40**, 1824–1832, <https://doi.org/10.1109/TGRS.2002.802519>.
- Knyazikhin, Y., J. V. Martonchik, R. B. Myneni, D. J. Diner, and S. W. Running, 1998: Synergistic algorithm for estimating vegetation canopy leaf area index and fraction of absorbed photosynthetically active radiation from MODIS and MISR data. *J. Geophys. Res.*, **103**, 32 257–32 274, <https://doi.org/10.1029/98JD02462>.
- , and Coauthors, 1999: MODIS leaf area index (LAI) and fraction of photosynthetically active radiation absorbed by vegetation (FPAR) product (MOD15). Algorithm Theoretical Basis Doc., 130 pp., [https://modis.gsfc.nasa.gov/data/atbd/atbd\\_mod15.pdf](https://modis.gsfc.nasa.gov/data/atbd/atbd_mod15.pdf).
- Kumar, S. V., and Coauthors, 2006: Land information system: An interoperable framework for high resolution land surface modeling. *Environ. Modell. Software*, **21**, 1402–1415, <https://doi.org/10.1016/j.envsoft.2005.07.004>.
- , R. H. Reichle, C. D. Peters-Lidard, R. D. Koster, X. Zhan, W. T. Crow, J. B. Eylander, and P. R. Houser, 2008: A land surface data assimilation framework using the land information system: Description and applications. *Adv. Water Resour.*, **31**, 1419–1432, <https://doi.org/10.1016/j.advwatres.2008.01.013>.
- Kurkowski, N. P., D. J. Stensrud, and M. E. Baldwi, 2003: Assessment of implementing satellite-derived land cover data in the Eta model. *Wea. Forecasting*, **18**, 404–416, [https://doi.org/10.1175/1520-0434\(2003\)18<404:AOISDL>2.0.CO;2](https://doi.org/10.1175/1520-0434(2003)18<404:AOISDL>2.0.CO;2).
- McNaughton, K. J., and T. W. Spriggs, 1986: A mixed-layer model for regional evaporation. *Bound.-Layer Meteor.*, **34**, 243–262, <https://doi.org/10.1007/BF00122381>.
- Miller, J., M. Barlage, X. Zeng, H. Wei, K. Mitchell, and D. Tarpley, 2006: Sensitivity of the NCEP/Noah land surface model to the MODIS green vegetation fraction data set. *Geophys. Res. Lett.*, **33**, L13404, <https://doi.org/10.1029/2006GL026636>.
- Myneni, R. B., and D. L. Williams, 1994: On the relationship between FAPAR and NDVI. *Remote Sens. Environ.*, **49**, 200–211, [https://doi.org/10.1016/0034-4257\(94\)90016-7](https://doi.org/10.1016/0034-4257(94)90016-7).
- Norman, J. M., W. P. Kustas, and K. S. Humes, 1995: A two-source approach for estimating soil and vegetation energy fluxes from observations of directional radiometric surface temperatures. *Agric. For. Meteorol.*, **77**, 263–293, [https://doi.org/10.1016/0168-1923\(95\)02265-Y](https://doi.org/10.1016/0168-1923(95)02265-Y).
- Peters-Lidard, C. D., and Coauthors, 2015: Integrated modeling of aerosol, cloud, precipitation and land processes at satellite-resolved scales. *Environ. Modell. Software*, **67**, 149–159, <https://doi.org/10.1016/j.envsoft.2015.01.007>.
- Quiring, S. M., 2011: Building the North American Soil Moisture (NASM) database. *2011 Fall Meeting*, San Francisco, CA, Amer. Geophys. Union, Abstract GC33C-02.
- Ruhge, R. L., and M. Barlage, 2011: Integrating a real-time green vegetation fraction (GVF) product into the land information system (LIS). *15th Symp. on Integrated Observing and Assimilation Systems for Atmosphere, Oceans, and Land Surface*, Seattle, WA, Amer. Meteor. Soc., J14.4, <https://ams.confex.com/ams/91Annual/webprogram/Paper182739.html>.
- Tanaka, S., K. Kawamura, M. Maki, Y. Muramoto, K. Yoshida, and T. Akiyama, 2015: Spectral index for quantifying leaf area index of winter wheat by field hyperspectral measurements: A case study in Gifu Prefecture, central Japan. *Remote Sens.*, **7**, 5329, <https://doi.org/10.3390/rs70505329>.
- Wittich, K.-P., 1997: Some simple relationships between land-surface emissivity, greenness and the plant cover fraction for use in satellite remote sensing. *Int. J. Biometeorol.*, **41**, 58–64, <https://doi.org/10.1007/s004840050054>.
- Xia, Y., and Coauthors, 2012a: Continental-scale water and energy flux analysis and validation for the North American Land Data Assimilation System project phase 2 (NLDAS-2): 1. Intercomparison and application of model products. *J. Geophys. Res.*, **117**, D03109, <https://doi.org/10.1029/2011JD016048>.



- , and Coauthors, 2012b: Continental-scale water and energy flux analysis and validation for North American Land Data Assimilation System project phase 2 (NLDAS-2): 2. Validation of model-simulated streamflow. *J. Geophys. Res.*, **117**, D03110, <https://doi.org/10.1029/2011JD016051>.
- Yin, J., X. Zhan, Y. Zheng, C. R. Hain, M. Ek, J. Wen, L. Fang, and J. Liu, 2016: Improving Noah land surface model performance using near real time surface albedo and green vegetation fraction. *Agric. For. Meteorol.*, **218-219**, 171–183, <https://doi.org/10.1016/j.agrformet.2015.12.001>.
- Zeng, X., P. Rao, R. S. DeFries, and M. C. Hansen, 2003: Interannual variability and decadal trend of global fraction vegetation cover from 1982 to 2000. *J. Appl. Meteor.*, **42**, 1525–1530, [https://doi.org/10.1175/1520-0450\(2003\)042<1525:IVADTO>2.0.CO;2](https://doi.org/10.1175/1520-0450(2003)042<1525:IVADTO>2.0.CO;2).